Title	Study on use of superconducting magnet and first inelastic neutron scattering experiment under magnetic field at 4SEASONS spectrometer
Author(s)	Kajimoto Ryoichi, Ishikado Motoyuki, Kira Hiroshi, Kaneko Koji, Nakamura Mitsutaka, Kamazawa Kazuya, Inamura Yasuhiro, Ikeuchi Kazuhiko, Iida Kazuki, Murai Naoki, Kawamura Seiko, Takahashi Ryuta, Aoyama Kazuhiro, Kambara Wataru
Citation	Physica B; Condensed Matter,556,p.26-30
Text Version	Accepted Manuscript
URL	https://jopss.jaea.go.jp/search/servlet/search?5063093
DOI	https://doi.org/10.1016/j.physb.2018.11.065
Right	

Study on use of superconducting magnet and first inelastic neutron scattering experiment under magnetic field at 4SEASONS spectrometer

Ryoichi Kajimoto[a,*], Motoyuki Ishikado[b], Hiroshi Kira[b], Koji Kaneko[a,c], Mitsutaka Nakamura[a], Kazuya Kamazawa[b], Yasuhiro Inamura[a], Kazuhiko Ikeuchi[b], Kazuki Iida[b], Naoki Murai[a], Seiko Ohira-Kawamura[a], Ryuta Takahashi[a], Kazuhiro Aoyama[a], Wataru Kambara[a]

[a]*Materials and Life Science Division, J-PARC Center, Japan Atomic Energy Agency, Tokai, Ibaraki 319-1195, Japan*
[b]*Neutron Science and Technology Center, Comprehensive Research Organization for Science and Society, Tokai, Ibaraki 319-1106, Japan*
[c]*Materials Sciences Research Center, Japan Atomic Energy Agency, Tokai, Ibaraki 319-1195, Japan*

Abstract

Magnets are important for studying magnetism and are commonly used as sample environment devices of neutron scattering instruments. However, the the use of magnets was prevented at the time-of-flight direct-geometry neutron spectrometer 4SEASONS in Materials and Life Science Experimental Facility (MLF) at J-PARC, because the instrument is surrounded by iron components, and it is equipped with a piece of equipment operated with magnetic bearings. In the present work, we investigate the influence of stray magnetic fields from a superconducting magnet which is shared among neutron scattering instruments in MLF. Based on the investigation, we modified 4SEASONS such that it can be used with the magnet. Finally, we successfully performed the first inelastic neutron scattering experiments with applied magnetic fields using this sample environment.

Keywords: J-PARC, Materials and Life Science Experimental Facility, 4SEASONS, Time-of-flight direct-geometry spectrometer, Superconducting magnet

1. Introduction

In neutron scattering experiment facilities, sample environments are as important as neutron scattering instruments. Cryostats that can cool samples to around the liquid helium temperature are the most popular sample environment (SE) devices. The need to realize more extreme conditions has arisen with the progress of material science, and larger or more complicated SE devices have been introduced in facilities. In the Materials and Life Science Experimental Facility (MLF) at the Japan Proton Accelerator Research Complex (J-PARC), the MLF-SE group prepared SE devices that are difficult for each instrument to maintain and are shared among instruments in MLF. Examples of such devices include a ^{3}He refrigerator, 2-K cryostats, a dilution refrigerator, a furnace, and a superconducting magnet [1].

The inelastic neutron scattering instrument 4SEASONS has a 4-K closed-cycle refrigerator as a standard SE device [2]. Moreover, we are developing the instrument to diversify the available SEs. One of the most important devices for our instrument is a magnet because a large proportion of the experiments performed using 4SEASONS is related to magnetism. To operate magnetic devices, it is desirable to construct the instrument with non-magnetic materials. Indeed, recent neutron scattering instruments have adopted stainless steel to build instrument components that are to be installed around the sample position [3–6]. However, stainless steel is more expensive compared to normal steel, and it increases the cost of constructing large components such as large vacuum scattering chambers, and at times, one cannot help using normal magnetic steel. This is the case for 4SEASONS. In this instrument, many components surrounding the sample area are made of iron. Moreover, large turbomolecular pumps (TMPs) with magnetic bearings are attached just below the sample position. The Fermi chopper used to monochromatize the incident beam has magnetic bearings as well, although it is located 1.7 m away from the sample. These components of the instrument constrain magnet operation at the instrument.

Accordingly, in this paper, we report the steps implemented to facilitate use of MLF-SE superconducting magnet on 4SEASONS. We estimated the influence of the stray field from the magnet by performing calculations and conducting magnet operation tests. We found that the TMPs pose the most severe constraint and relocated them to facilitate magnet usage. Finally, we successfully performed an experiment with applied magnetic fields, although we limited the maximum applied field at the instrument.

2. Sample area of 4SEASONS and calculation model

4SEASONS is a time-of-flight direct-geometry neutron spectrometer for inelastic neutron scattering experiments using thermal neutrons, and it is installed on the BL01 beamline at MLF [2, 7, 8]. Fig. 1 shows a transverse section of 4SEASONS along the beam path (before relocation of the TMPs, as described later).

*Corresponding author
Email address: ryoichi.kajimoto@j-parc.jp (Ryoichi Kajimoto)

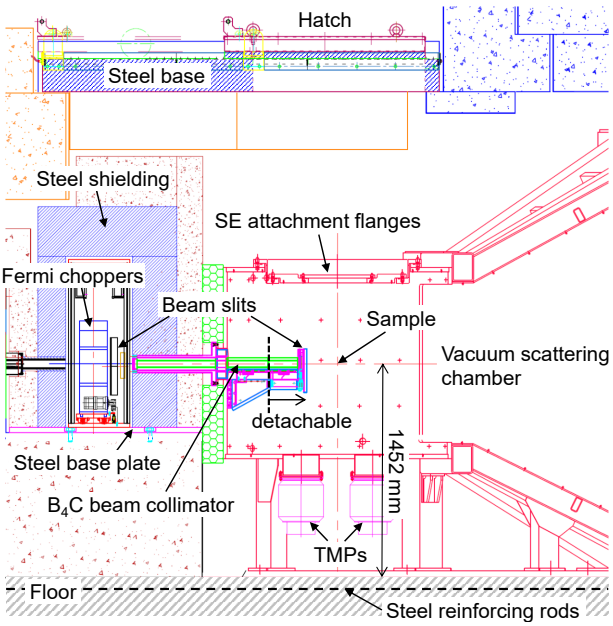

Figure 1: Side view of 4SEASONS around the sample position.

The sample position is 1452 mm above the floor of the experimental hall [9]. The sample and the detectors are enclosed in a large vacuum scattering chamber. The downstream end of the vacuum scattering chamber houses ^{3}He position-sensitive detector tubes, and the distance between the sample and the detector is 2.5 m. The vacuum scattering chamber consists of stainless-steel walls and steel beams. The vacuum scattering chamber is equipped with three concentric flanges for installing SE devices above the sample position. These flanges are made of stainless steel, and their dimensions are compatible with JIS (Japanese Industrial Standards) 400-mm, 800-mm, and 1000-mm flanges. The 400-mm and 800-mm flanges are defined as the standard SE attachment flanges in MLF [1]. Two sets of four-quadrant motorized beam slits located upstream of the sample define the beam size. The downstream set of slits is located at the end of a B_4C beam collimator, which is 256 mm upstream of the sample. This set of slits and the end part of the collimator are detachable. The vacuum scattering chamber has three evacuation ports at the bottom, whose flanges have a nominal diameter of 250 mm. One of them is connected to a roughing pump. Two vertically oriented TMPs are attached directly to the other two ports. They are used in combination with the roughing pump and a cryopump to realize cryogenic vacuum in the vacuum scattering chamber (Only one of them is operated, and the other is kept as a spare.). Two different types of Fermi choppers are installed 1.7 m upstream of the sample to monochromatize the incident neutron beam [10]. They are mounted on a translation stage that is fixed on a 35-mm-thick base plate, and they are surrounded by a thick steel shielding. The vacuum scattering chamber is housed in a concrete shielding house, and the SE devices are loaded through a hatch above the sample position. The hatch lid is made of a combination of a 50-mm-thick steel plate and a plate of boric acid, and it is mounted on a 230-mm-thick steel base. The entire floor of the experimental hall is reinforced with steel rods measuring 35 mm in diameter, and these rods are buried ~80 mm under the floor.

The MLF-SE magnet is a vertical field superconducting magnet with split-pair coils, and its maximum available magnetic field is 7 T [1]. It is equipped with a JIS 800-mm flange, and the diameter of the outer vacuum chamber is ~700 mm. This magnet is installed on 4SEASONS by attaching it to the 800-mm flange, and the detachable part of the B_4C collimator and the downstream set of the four-quadrant beam slits are removed.

The stray fields and forces induced by the MLF-SE 7 T superconducting magnet were calculated by using the computer-aided engineering system Femtet® [11]. To test our magnet model, we calculated the magnitude of the stray field along the horizontal direction as a function of distance. We confirmed that the obtained values coincided well with those provided by the magnet manufacturer. Then, we built a model including the vacuum scattering chamber, steel shielding around the Fermi chopper, steel part of the hatch and its base, and steel reinforcing rods under the floor. The reinforcing rods are arranged in a grid pattern, but we replaced them with a steel plate to simplify the model. We ignored other components such as concrete shields, and assumed they are filled with air. To calculate the magnetic properties of metal components, we used the magnetization curve data of JIS SS400 [12] and JIS SUS304 for steel and stainless steel, respectively. These are the typically used iron materials in Japan.

3. Study of stray fields

First, we investigated the effects of the steel components on the magnet. The stray field around the sample position is attenuated by the steel components because they absorb magnetic flux. The steel components are magnetized by the stray field, and they may remain magnetized even when the applied magnetic field is switched off. According to our calculation, when the applied magnetic field H is 7 T, the magnetized steel beams of the scattering chamber induce a magnetic field of ~30 G at the sample position. However, the remanent magnetization can be reduced by lowering H to zero while oscillating the direction of the field. In our test operation of the magnet, which is described later, the remanent magnetic field on the surfaces of steel components after demagnetization was less than 1 G. Another problem caused by the steel components is that they attract the coils in the magnet during operation. Because the coils are arranged vertically in this vertical-field magnet, any extraordinarily strong force on the coils along the horizontal direction may damage the magnet. Accordingly, we estimated the forces exerted on the coils by calculation. We found the total magnitude of the forces to be ~190 N at H = 7 T. This force is smaller than the force generated between the coils by three to four orders of magnitude. The horizontal component of the force was estimated to be 180 N. We do not have the exact criteria for the horizontal force on the coils, but the magnet has occasionally been operated on another beamline at an inclination of ~5°. In this situation, approximately 10% of the coil weight is applied horizontally on the coils. Because the total weight of

the coils is approximately 200 kg, the magnet has been operated safely with a horizontal force of ~200 N. The estimated magnitude of force along the horizontal direction was lower than this value, even at the maximum applied field of 7 T. Therefore, we concluded that the force between the steel components and the magnet coils is not a problem.

Next, we investigated the effect of the stray field on devices that may be damaged by magnetic fields. We considered two types of key components in the instrument: the Fermi choppers and the TMPs. As described in the previous section, the Fermi choppers are 1.7 m away from the sample. The magnitude of the field at the same distance from the magnet is ~20 G at $H = 7$ T, which is considerably smaller than the acceptable value for the Fermi chopper (~0.4 T). In reality, the magnitude of the field is smaller than this value because the steel shielding around the Fermi choppers absorbs magnetic flux. Our calculation showed that the magnitude of the magnetic field at the Fermi choppers was ~0.25 G, which is harmless.

The last and most important issue we considered is the effect of the stray field on the TMPs. According to the TMP vendor, the magnitude of the magnetic field at the TMP should be less than 150 G and 50 G along the axial direction and the direction perpendicular to the rotation axis, respectively, when the TMPs are stationary and not in use. When the TMPs are operated under the magnetic field, the condition becomes more severe. Because the MLF-SE 7 T magnet can be operated with its own outer vacuum chamber to maintain a high vacuum, we can use the magnet without operating the TMPs. Consequently, we tried to find the condition that satisfies the criteria of 150 G and 50 G.

To check the accuracy of our calculation, we compared the calculated and observed values of the stray field at low H values. The magnitude of the magnetic field was measured using a gaussmeter. Fig. 2(a) shows the calculated spatial distribution of the absolute value of the magnetic field at $H = 1$ T around the TMP attachment flange at the bottom of the vacuum scattering chamber. Because the sample position, that is, the center of the magnet, was located at $y = +250$ mm, the magnitude of the magnetic field increased as y increased. We then installed the magnet on 4SEASONS [Fig. 3(a)] and operated it at $H \leq 1$ T [10]. Fig. 4(a) shows the observed absolute value of the magnetic field at the center of the attachment flange [marked by a cross in Fig. 2(a)]. The value increases linearly as a function of H, and reaches 51 G at $H = 1$ T. The latter value is consistent with the calculated value of ~40 G [Fig. 2(a)].

The easiest way to reduce the stray field at the TMP positions is to place the TMPs away from the magnet. However, bending the exhaust route between the vacuum scattering chamber and the TMPs causes a loss of evacuating power. To reduce the loss of evacuating power to the extent possible, the exhaust route should be kept straight. Another way to reduce the stray field is to surround the TMPs with high-permeability magnetic alloys. We investigated the size and thickness of permalloy cover surrounding the TMPs to sufficiently reduce the magnetic field. However, we found that the required thickness was too excessive, and such a thick cover would make it difficult to maintain the TMPs. Therefore, we studied a case in which the TMPs are moved downward from their original positions.

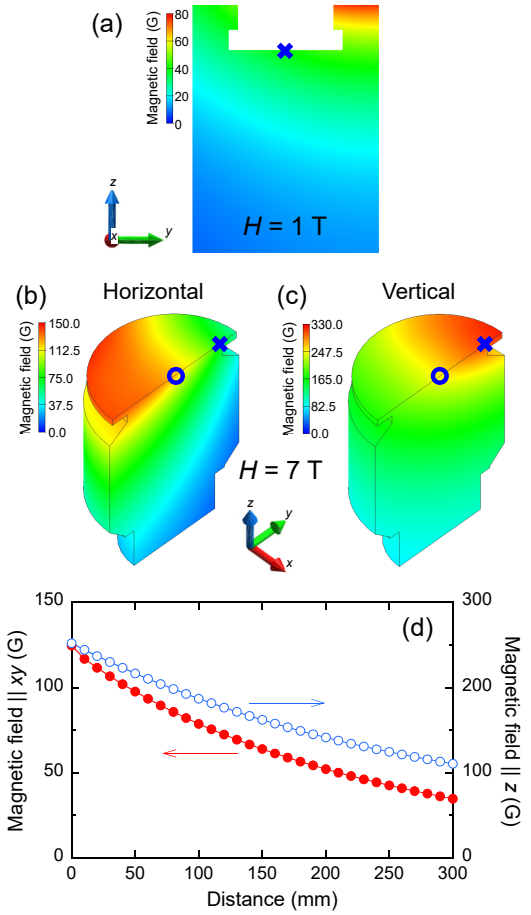

Figure 2: (a)–(c) Calculated distributions of stray magnetic field around a TMP of 4SEASONS. The z direction corresponds to the vertical direction, and the y direction is parallel to the incident neutron beam. The center axis of the magnet is located at $y = +250$ mm relative to the center of the TMP. (a) Magnetic field in the area around the attachment flange of the TMP on the vacuum scattering chamber (denoted by the white area) at $H = 1$ T. (b) and (c) Vertical and horizontal components of the magnetic field in the TMP, respectively, at $H = 7$ T. (d) Calculated magnetic field at the flange center [denoted by circles in (b) and (c)] as a function of the TMP position when $H = 7$ T. The closed and open symbols denote the values of the horizontal and vertical components, respectively.

Herein, we investigate the stray magnetic field by decomposing it into horizontal and vertical components. Figs. 2(b) and 2(c) show the calculated spatial distributions of the horizontal and vertical components of the magnetic field, respectively, near one of the TMPs at $H = 7$ T. The central axis of the magnet is located at $y = +250$ mm relative to the TMP center. The magnitude of the vertical component is significantly higher than that of the horizontal component, and it increases as the position becomes closer to the magnet. By contrast, the horizontal component intensifies as the position becomes farther from the magnet. This difference in the position dependence is due to the spatial distribution of the magnetic flux from the vertical magnet. Fig. 2(d) shows the magnitudes of the horizontal and vertical components of the magnetic field as the position of the TMP moves downward. It shows the values at the center of the

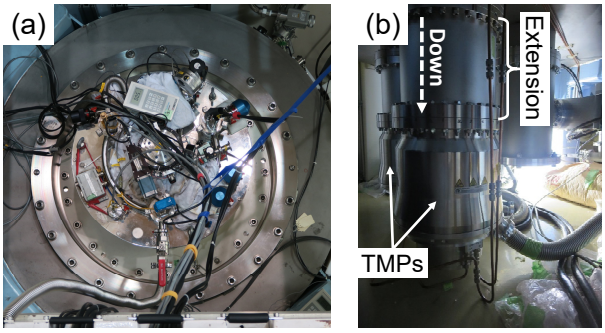

Figure 3: (a) The MLF-SE 7 T superconducting magnet installed in the sample environment flange of 4SEASONS. (b) TMPs attached to the 250-mm extensions below the vacuum scattering chamber of 4SEASONS.

top flange of the TMP [marked by circles in Fig. 2(b) and 2(c)] as a function of the moving distance of the TMP relative to its original position. The magnitudes of both components decrease as the TMP moves farther from the magnet. Fig. 2(d) suggests that if we move the TMP downward by ∼250 mm, the magnetic field can be reduced to the values allowed for the TMP, even at $H = 7$ T.

4. Modification of instrument

Based on the above investigations, we upgraded the instrument. We introduced an extension pipe between the TMPs and the flanges on the vacuum scattering chamber to relocate the TMPs 250 mm downward relative to their original positions [Fig. 3(b)]. Subsequently, we operated the MLF-SE 7 T magnet on 4SEASONS and measured the magnetic field on the flange of one of the TMPs. Fig. 4(b) shows the observed magnetic field as a function of H. The horizontal and vertical components of the magnetic field were measured at a position on the TMP flange closest to the magnet [marked by crosses in Figs. 2(b) and (c)]. The magnitude of the magnetic field increases in proportion to the value of H. The values of the horizontal and vertical components, and the absolute magnitude at $H = 3.5$ T are 30.4 G, 59.9 G, and 67.1 G, respectively. Our calculations suggest that the magnitude of the horizontal component at the center of the TMP flange is 1.8 times greater than that at the observed position. Therefore, we decided to limit the maximum applied field at 4SEASONS to 3 T for safety, because the horizontal magnetic field at the center of the flange may reach the criterion of 50 G at this applied field.

By contrast, the calculated values at the same H and position are 11.7 G (horizontal component), 70.9 G (vertical component), and 71.8 G (absolute magnitude). The absolute magnitude and the vertical component of the observed magnetic field agree well with the calculated values, but the horizontal component is significantly greater than the calculated value. Considering that the absolute magnitude shows good coincidence, one of the possible origins of the difference in the horizontal component is the inclination of the gaussmeter probe. The horizontal component is especially sensitive to inclination of the probe, because it is significantly smaller than the vertical component. We found that the inclination of ∼17° helps achieve

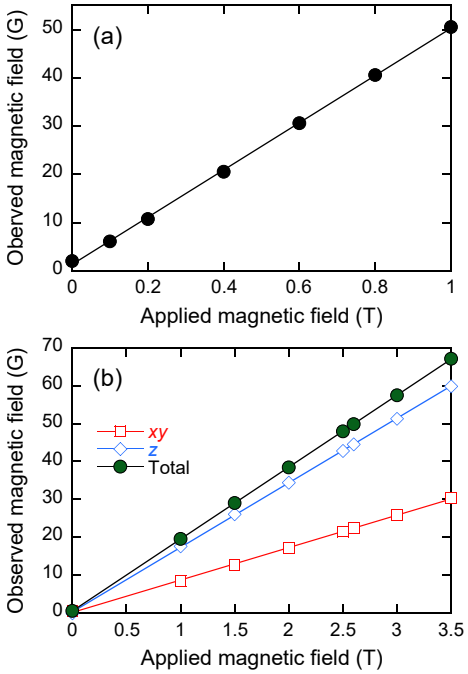

Figure 4: (a) Observed magnetic field at top-center of attachment flange [marked by cross in Fig. 2(a)] as a function of applied magnetic field. (b) Observed magnetic fields at the edge of the attachment flange closest to the magnet [marked by crosses in Figs. 2(b) and (c)] after relocation of the TMPs. Solid symbols denote the total magnitude of the magnetic field, and the open squares and open diamonds denote the horizontal and vertical components, respectively. In all panels, the solid lines indicate linear fits.

good agreement between the observed and calculated values. Although this angle seems too large, it is reasonable to consider the inclination of the probe is the major cause of the difference. Moreover, the magnetization of parts of the TMPs can be reduced by demagnetization during shutdown of the magnet, which may increase the allowed magnetic field to a value greater than that specified in the nominal criteria. Based on these considerations, magnet operation at $H = 7$ T should be feasible at 4SEASONS. Although we decided to limit the maximum applied field at 4SEASONS to 3 T for safety, the limit may be relaxed in the future by reexamining the magnetic field acting on the TMPs.

5. On-beam test using a real sample

After the abovementioned works, we finally carried out a neutron scattering experiment with a real sample under magnetic fields by using 4SEASONS. To control the magnet remotely, we introduced a driver software component for the magnet into the IROHA2-based instrument control system of 4SEASONS [13]. For this demonstration measurement, we employed a single crystal of TbB_2C_2. This compound is known to exhibit antiferroquadrupolar ordering under magnetic fields [14–17]. A previous inelastic neutron scattering study by Mulders et al. using a powder sample of TbB_2C_2 reported that magnetic excitation appears around 3.5 meV at low temperatures, and it shifts toward higher energies under applied magnetic field of the order of 1 T [18]. Therefore, this compound is suitable for our

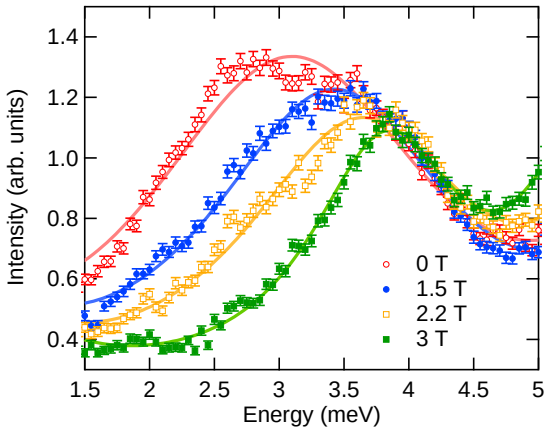

Figure 5: Powder-averaged inelastic neutron scattering profiles of $Tb^{11}B_2C_2$ at 4 K as a function of energy transfer. Open circles, closed circles, open squares, and closed squares denote the data measured under 0, 1.5, 2.2, and 3 T. Solid lines are guides to the eye.

experiment under low magnetic fields. A ~300 mg single crystal of $Tb^{11}B_2C_2$ was grown with the Czochralski method by using a tetra-arc furnace. To reduce neutron absorption, we used enriched ^{11}B. The crystal was aligned to have the $(h, 0, l)$ horizontal scattering plane, and a magnetic field was applied along the [010] direction. The crystal was attached to the end of the center stick of the magnet and was cooled to 4 K. An incident energy of 10 meV was selected by rotating the Fermi chopper at 200 Hz. The scattered neutron intensity was measured with rotating the sample horizontally over 97° in steps of 1°. The data were converted into the scattering function $S(Q, E)$ and were powder-averaged by using the software package Utsusemi [19] for comparison with the powder data in Ref. [18]. Because the vertical aperture of the magnet was ±10° relative to the sample, we masked the data out of this angular range in the powder-averaging process.

Fig. 5 shows the magnetic excitation spectra sliced in the range of Q = 1.5–2 Å^{-1} under applied magnetic fields with the data of the zero field. At H = 0 T, we observed a broad excitation peak around 3 meV. As H increased, the peak sharpened and changed its position toward higher energies. These observations reproduce well the results in Ref. [18], although the peak position at 3 T, 3.8 meV, is slightly lower than the value reported in Ref. [18] (4.1 meV). The difference may have originated from the imperfect powder-averaging using the single-crystal data and the strong magnetic anisotropy of TbB_2C_2 [14, 17]. The first magnetic field experiment at 4SEASONS was thus successful.

However, we found that the intensity of background scattering was higher as compared to that in experiments using the standard cryostat, although we used an oscillating radial collimator dedicated for the magnet. The background was especially high in the small scattering angle region, and fortunately, we could avoid this region to produce the data shown in Fig. 5. However, in general, this background would be a problem. One of the probable causes of the high background is that we removed the end part of the beam collimator and the downstream set of beam slits to install the magnet. This causes a severe increase in unwanted scattering from the thick aluminum walls and the complex components inside the magnet, despite the use of the radial collimator. We are developing a new set of beam slits operated by ultrasonic motors, which are usable under magnetic fields. We expect that these slits will reduce the background scattering caused by the magnet.

6. Summary

We investigated the influence of the stray magnetic field from the MLF-SE 7 T superconducting magnet on the 4SEASONS spectrometer by considering iron components and devices operated with magnetic bearings such as TMPs and Fermi choppers. We found that the most serious issue is the influence of the magnetic field on the TMPs. Based on the investigation, we relocated the TMPs downward by 250 mm. Finally, we performed the first inelastic neutron scattering experiment under magnetic fields by using a single crystal of $Tb^{11}B_2C_2$. The observed field dependence of the magnetic excitation spectrum was consistent with a previous report, which proved the experiment was successful.

Acknowledgments

We greatly acknowledge technical support of the MLF-SE group and the engineers of the Neutron Science Section and the Technology Development Section of MLF. The proposal number of the neutron scattering experiment in MLF is 2018I0001.

References

[1] S. Ohira-Kawamura, T. Oku, M. Watanabe, R. Takahashi, K. Munakata, S. Takata, Y. Sakaguchi, M. Ishikado, K. Ohuchi, T. Hattori, H. Kira, K. Sakai, T. Aso, Y. Yamauchi, S. Isomae, Sample environment at the J-PARC MLF, J. Neutron Res. 19 (2017) 15–22. doi:10.3233/JNR-170046.

[2] R. Kajimoto, M. Nakamura, Y. Inamura, F. Mizuno, K. Nakajima, S. Ohira-Kawamura, T. Yokoo, T. Nakatani, R. Maruyama, K. Soyama, K. Shibata, K. Suzuya, S. Sato, K. Aizawa, M. Arai, S. Wakimoto, M. Ishikado, S. Shamoto, M. Fujita, H. Hiraka, K. Ohoyama, K. Yamada, C.-H. Lee, The Fermi chopper spectrometer 4SEASONS at J-PARC, J. Phys. Soc. Jpn. 80 (2011) SB025. doi:10.1143/JPSJS.80SB.SB025.

[3] R. I. Bewley, J. W. Taylor, S. M. Bennington, LET, a cold neutron multi-disk chopper spectrometer at ISIS, Nucl. Instrum. Methods Phys. Res., Sect. A 637 (2011) 128–134. doi:https://doi.org/10.1016/j.nima.2011.01.173.

[4] T. Yokoo, K. Ohoyama, S. Itoh, K. Iwasa, N. Kaneko, J. Suzuki, M. Ohkawara, K. Aizawa, S. Tasaki, T. Ino, K. Taketani, S. Ishimoto, M. Takeda, T. Oku, H. Kira, K. Hayashi, H. Kimura, T. J. Sato, Polarized neutron spectrometer for inelastic experiments at J-PARC—status of POLANO project, EPJ Web Conf. 83 (2015) 03018. doi:10.1051/epjconf/20158303018.

[5] G. Ehlers, A. A. Podlesnyak, A. I. Kolesnikov, The cold neutron chopper spectrometer at the Spallation Neutron Source—a review of the first 8 years of operation, Rev. Sci. Instrum. 87 (2016) 093902. doi:10.1063/1.4962024.

[6] M. Russina, G. Guenther, V. Grzimek, R. Gainov, M.-C. Schlegel, L. Drescher, T. Kaulich, W. Graf, B. Urban, A. Daske, K. Grotjahn, R. Hellhammer, G. Buchert, H. Kutz, L. Rossa, O.-P. Sauer, M. Fromme, D. Wallacher, K. Kiefer, B. Klemke, N. Grimm, S. Gerischer, N. Tsapatsaris, K. Rolfs, Upgrade project NEAT'2016 at Helmholtz Zentrum Berlin—what can be done on the medium power neutron source, Physica B in press. doi:10.1016/j.physb.2017.12.026.

[7] H. Seto, S. Itoh, T. Yokoo, H. Endo, K. Nakajima, K. Shibata, R. Kajimoto, S. Ohira-Kawamura, M. Nakamura, Y. Kawakita, H. Nakagawa, T. Yamada, Inelastic and quasi-elastic neutron scattering spectrometers in J-PARC, Biochim. Biophys. Acta, Gen. Subj. 1861 (2017) 3651–3660. doi:10.1016/j.bbagen.2016.04.025.

[8] K. Nakajima, Y. Kawakita, S. Itoh, J. Abe, K. Aizawa, H. Aoki, H. Endo, M. Fujita, K. Funakoshi, W. Gong, M. Harada, S. Harjo, T. Hattori, M. Hino, T. Honda, A. Hoshikawa, K. Ikeda, T. Ino, T. Ishigaki, Y. Ishikawa, H. Iwase, T. Kai, R. Kajimoto, T. Kamiyama, N. Kaneko, D. Kawana, S. Ohira-Kawamura, T. Kawasaki, A. Kimura, R. Kiyanagi, K. Kojima, K. Kusaka, S. Lee, S. Machida, T. Masuda, K. Mishima, K. Mitamura, M. Nakamura, S. Nakamura, A. Nakao, T. Oda, T. Ohhara, K. Ohishi, H. Ohshita, K. Oikawa, T. Otomo, A. Sano-Furukawa, K. Shibata, T. Shinohara, K. Soyama, J. Suzuki, K. Suzuya, A. Takahara, S. Takata, M. Takeda, Y. Toh, S. Torii, N. Torikai, N. L. Yamada, T. Yamada, D. Yamazaki, T. Yokoo, M. Yonemura, H. Yoshizawa, Materials and Life Science Experimental Facility (MLF) at the Japan Proton Accelerator Research Complex II: Neutron scattering instruments, Quantum Beam Sci. 1 (2017) 9. doi:10.3390/qubs1030009.

[9] Neutron Facility Group (Ed.), J-PARC Materials and Life Science Facility experimental apparatus installation manual (edition 1), JAERI-Tech 2004-059, Japan Atomic Energy Research Institute, [in Japanese] (2004). doi:10.11484/jaeri-tech-2004-059.

[10] R. Kajimoto, M. Nakamura, Y. Inamura, K. Kamazawa, K. Ikeuchi, K. Iida, M. Ishikado, N. Murai, H. Kira, T. Nakatani, S. Ohira-Kawamura, R. Takahashi, N. Kubo, W. Kambara, K. Nakajima, K. Aizawa, Status report of the chopper spectrometer 4SEASONS, J. Phys.: Conf. Ser. 1021 (2018) 012030. doi:10.1088/1742-6596/1021/1/012030.

[11] Murata Software Co., Ltd., https://www.muratasoftware.com/en/.

[12] The Japan Welding Engineering Society, http://www-it.jwes.or.jp/qa/details.jsp?pg_no=0030030100, [in Japanese].

[13] T. Nakatani, Y. Inamura, T. Ito, K. Moriyama, IROHA2: Standard instrument control software framework in MLF, J-PARC, in: NOBUGS 2016 Proceedings, 2016, pp. 76–79. doi:10.17199/NOBUGS2016.70.

[14] K. Kaneko, H. Onodera, H. Yamauchi, K. Ohoyama, A. Tobo, Y. Yamaguchi, Anomalous antiferromagnetic properties of the tetragonal compound, TbB_2C_2, J. Phys. Soc. Jpn. 70 (2001) 3112–3118. doi:10.1143/JPSJ.70.3112.

[15] K. Kaneko, S. Katano, M. Matsuda, K. Ohoyama, H. Onodera, Y. Yamaguchi, Neutron-scattering studies of the field-induced ordered state of TbB_2C_2, Appl. Phys. A 74 (2002) S1749–S1751. doi:10.1007/s003390101268.

[16] K. Kaneko, K. Ohoyama, S. Katano, M. Matsuda, H. Onodera, Y. Yamaguchi, Anomalous magnetic ordering phenomena in tetragonal TbB_2C_2 observed by neutron diffraction, J. Phys. Soc. Jpn. 71 (2002) 3024–3029. doi:10.1143/JPSJ.71.3024.

[17] K. Kaneko, H. Onodera, H. Yamauchi, T. Sakon, M. Motokawa, Y. Yamaguchi, Magnetic phase diagrams with possible field-induced antiferroquadrupolar order in TbB_2C_2, Phys. Rev. B 68 (2003) 012401. doi:10.1103/PhysRevB.68.012401.

[18] A. Mulders, U. Staub, O. Zaharko, S. Janssen, Magnetic field-induced orbital order in TbB_2C_2 observed by inelastic neutron scattering, Physica B 359-361 (2005) 1231–1233. doi:10.1016/j.physb.2005.01.367.

[19] Y. Inamura, T. Nakatani, J. Suzuki, T. Otomo, Development status of software "Utsusemi" for chopper spectrometers at MLF, J-PARC, J. Phys. Soc. Jpn. 82 (2013) SA031. doi:10.7566/JPSJS.82SA.SA031.